Microgravity Sci. Technol. (2011) 23:191–197
DOI 10.1007/s12217-010-9249-y

ORIGINAL ARTICLE

# Parabolic Flights @ Home

## An Unmanned Air Vehicle for Short-Duration Low-Gravity Experiments

**Paul Gerke Hofmeister · Jürgen Blum**

Received: 1 November 2009 / Accepted: 3 November 2010 / Published online: 23 November 2010


**Abstract** We developed an unmanned air vehicle (UAV) suitable for small parabolic-flight experiments. The flight speed of 100 m $s^{-1}$ is sufficient for zero-gravity parabolas of 16 s duration. The flight path's length of slightly more than 1 km and 400 m difference in altitude is suitable for ground controlled or supervised flights. Since this fits within the limits set for model aircraft, no additional clearance is required for operation. Our UAV provides a cost-effective platform readily available for low-g experiments, which can be performed locally without major preparation. A payload with a size of up to $0.9 \times 0.3 \times 0.3$ $m^3$ and a mass of ∼5 kg can be exposed to 0 $g_0$–5 $g_0$, with $g_0$ being the gravitational acceleration of the Earth. Flight-duration depends on the desired acceleration level, e.g. 17 s at 0.17 $g_0$ (lunar surface level) or 21 s at 0.38 $g_0$ (Martian surface level). The aircraft has a mass of 25 kg (including payload) and a wingspan of 2 m. It is powered by a jet engine with an exhaust speed of 450 m $s^{-1}$ providing a thrust of 180 N. The parabolic-flight curves are automated by exploiting the advantages of sophisticated micro-electronics to minimize acceleration errors.

**Keywords** Parabolic flights · Unmanned aerial vehicle (UAV)

P. G. Hofmeister (✉) · J. Blum
Institut für Geophysik und extaterrestrische Physik,
Technische Universität zu Braunschweig,
Braunschweig, Germany
e-mail: p.hofmeister@tu-bs.de

J. Blum
e-mail: j.blum@tu-bs.de

### Introduction to Parabolic Flights

Various implemented concepts for the realization of microgravity exist, differing in duration and quality of the microgravity they provide as well as the availability for application (see Table 1). The latter is often limited to a low number of experiments in a given time frame. Laboratory microgravity experiments are limited to a duration of less than a few seconds, due to the finite free-fall height available in the laboratory. Drop towers provide slightly longer microgravity durations but the repeatability is usually limited to a few experiments per day. However, drop towers have been successfully used for all kinds of basic and applied research in the past decades (see, e.g., Dreyer 2010; Blum 2010). Commercial parabolic flights (Pletser 2004; Pletser et al. 2008) allow dozens of experiments per day but are not available throughout the year. However, they can accommodate rather large and heavy experimental equipment, and can also provide parabolas with a finite (e.g. Martian or Lunar) residual acceleration (Pletser et al. 2010). Suborbital flights and the International Space Station provide extended periods of microgravity time but are rather costly.

So far, small unmanned air vehicles (UAV) have not been used for microgravity experiments, due to the limited availability of powerful engines (Mesland 1995). To gain easier access to low gravity, we developed an UAV, which can be operated on a regular basis. Last decade's technological advances of the mass market for jet-powered model aircraft and micro computers pave the way for an effortless development at extremely competitive costs. Our development is based on a series aircraft from *UR-Modellbau*. Custom modifications for low-gravity flight consist of a specialized closed-loop

**Table 1** Comparison between different methods for the generation of low gravity

| Method | Duration [s] | Typical residual acceleration [$g_0$] | Typical payload mass per experiment [kg] | Reference |
|---|---|---|---|---|
| Laboratory free-fall experiments | $\lesssim$2 s | $10^{-2} \ldots 10^{-6}$ | $\lesssim$50 | Beitz (2010) |
| Drop tower facilities | $\lesssim$9 s | $10^{-5} \ldots 10^{-6}$ | $\lesssim$300 | ZARM Drop Tower Bremen User Manual, Rath (1995) |
| Parabolic flight @ home | $\lesssim$16 s | $\sim 10^{-1}$ | $\lesssim$5 | This work |
| Parabolic flight facilities | $\lesssim$25 s | $\sim 10^{-2}$ | $\lesssim$500 | Pletser (2004), Pletser et al. (2008) |
| Suborbital flights | $\lesssim$15 min | $10^{-3} \ldots 10^{-6}$ | $\lesssim$500 | Hamacher et al. (1987), Fitton and Seibert (2001) |
| ISS | $\lesssim$3 months | $10^{-3} \ldots 10^{-6}$ | $\lesssim$500 | Jules et al. (2004) |

controller and a zero-g-capable fuel system. Fully automated flight is currently not considered due to safety reasons. Required sensors are either too heavy-weight or do not offer the necessary precision to be used without correction. The cost would not be justified by the benefits.

A parabola-flight maneuver consists of an initial "pull-up" phase, in which the nose of the aircraft is lifted so that an increasing climb angle is reached. When the maximum climb angle is reached, the thrust of the engine is reduced to the level necessary to compensate air drag so that the aircraft follows the parabola of a free-fall flight path. During this parabola, the nose of the aircraft is tilting downwards until the maximum negative tilt angle is reached. Hereupon, the nose is pulled up again, which causes a strong acceleration inside the aircraft, until the flight path is horizontal again.

To describe the properties of the accelerated frame of reference within a parabolic-flight aircraft we start from a description of the general forces acting on the aircraft. Figure 1a shows an aircraft travelling at constant speed and altitude. The angle $\alpha$ between the airfoils and the velocity is the angle of attack. $F$ is the force created by the engine, $L$ is the aerodynamic lift perpendicular to the direction of motion, $D$ the drag anti-parallel to the direction of motion and $G$ is the weight towards the center of earth. At constant velocity the sum of these forces vanishes. The angle of attack depends on the position of the control surfaces. Lift $L$ and drag $D$ depend on the speed and the angle of attack $\alpha$.

Figure 1b shows the situation during weightlessness. The sum of all forces, i.e. thrust, lift, drag and weight equals weight. To achieve this, lift and, hence, angle of attack must vanish. In this flight condition thrust and lift are anti-parallel and their absolute values must be equal.

As shown in Fig. 1c, non-zero constant-$g$ flight is created by setting an appropriate angle of attack to achieve the desired acceleration as lift, while thrust counters drag. Due to the non-zero angle of attack, slightly less lift and slightly less thrust is required. However, the angle of attack is small enough for this effect to be negligible. As the experiment is rotating with the the aircraft, the acceleration is acting in the same direction throughout the parabola.

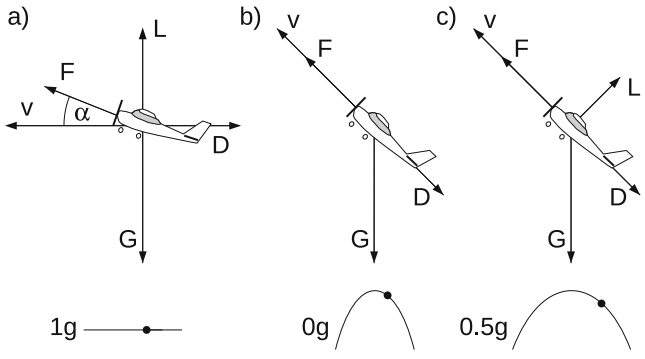


**Fig. 1** Forces acting on the aircraft during **a** horizontal (i.e. 1-$g$), **b** zero-$g$, **c** and low-$g$ flight. The curves in the lower part of the figure show where the depicted state is reached during the parabola

## Using Small UAVs for Parabolic Flights

Small UAVs can operate at almost any model-aircraft-field available in nearly every region. They can take-off and land on grass, asphalt or concrete runways of only 100 m lengths. Obviously, the operating cost of small aircraft is much lower than that of larger aircraft. Since the control response-time depends on the ratio of flight speed and rudder size, the response time of a small UAV is much faster than that of a large aircraft. The frequency of the control oscillations of small aircraft is much higher than that of larger aircraft. A frequency of 10 Hz leads to nearly no acceleration errors averaged

over short periods of time. The upper limit of acceleration for small aircraft normally is higher than those of lager aircraft. An experiment onboard our UAV can be run at 0.05 $g_0$ to 5 $g_0$ at one flight day without hardware changes. Here, $g_0 = 9.8$ m s$^{-2}$ is the gravitational acceleration of the Earth. Our UAV (see Section "The Delta-Wing with Canard Wings") has a maximum take-off weight (MTOW) of 24.99 kg, which means that only limited legal restrictions are imposed. In addition to that, an aircraft with a wingspan of 2 m does not require any specialized transportation equipment.

## Preliminary Tests

Preliminary tests were done with a very small UAV with a mass of 2 kg, powered by a piston-engine with a displacement of 7.5 cm$^3$ and allowing a speed of 40 m s$^{-1}$. The UAV was manually flown by remote control. During the parabola, the elevator was switched to a fixed position to reach an angle of attack of zero degrees. This leads to vanishing lifting force during the parabola. Perturbation and non-constant torque and forces require control as available on the new UAV. A typical example of an acceleration curve reachable in such a flight is shown in Fig. 2. Typical microgravity durations of ∼4 s and residual accelerations of ∼0.1 $g_0$ were easily reachable. These results motivated us to develop a somewhat larger UAV with an extended period of low gravity of up to 16 s and a payload mass of up to 5 kg (see below).

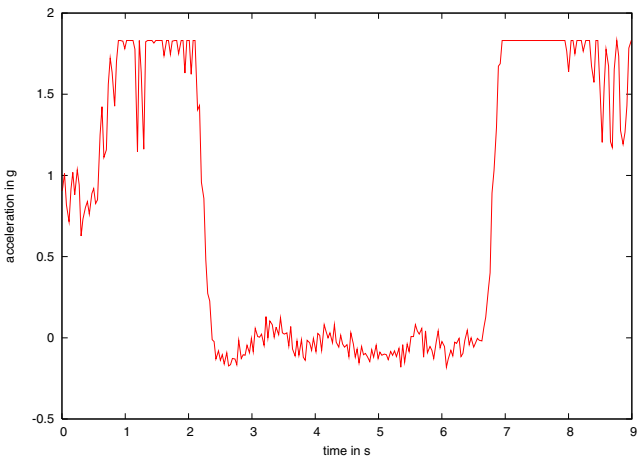


**Fig. 2** Example of the residual acceleration of a small UAV. This curve was obtained with a small propeller-engine aircraft with no acceleration control. Due to the low airspeed of 40 m s$^{-1}$, the low-gravity duration is short. Measurement errors are less than $2 \cdot 10^{-3}$ $g_0$

## Simulated Flight Paths

Available model aircraft allow maximum velocities of ∼100 m s$^{-1}$. In order to evaluate the prospects of such an aircraft for parabolic-flight purposes, we developed a simulation software, which enabled us to vary the initial speed of the aircraft, the acceleration during pull-up and under reduced-gravity condition, and the duration of the pull-up phase. The software does not take into account air drag, thus assuming that the aircraft will always compensate air drag by thrust. The flight path and the orientation of the aircraft reached under these ideal conditions were then simulated as a function of time. The model was validated in comparison to an analytically calculated trajectory at zero-g (no acceleration except gravity of the earth). Such simulations provide a good estimation of expected low-$g$ flight duration depending on the desired acceleration and given entry speed. The maximum temporal change of the inclination (and therefore the maximum angular rate) is reached at the top of the parabola, providing information about centrifugal forces during the parabola. As the duration of the microgravity phase, it depends on the acceleration during pull-up, the duration of the pull-up phase and the initial climb angle to the horizontal. A large initial climb angle leads to high maximum angular rate and long low-$g$ flight duration. In case of small pull-up accelerations (∼2 $g_0$) and large initial climb angles, the duration of the microgravity phase is almost unaffected by the initial climb angle, because the aircraft slows down too much before reaching the desired initial climb angle. In case of large accelerations (5 $g_0$) during the pull-up phase, larger initial climb angles increase the flight duration. A high initial climb angle leads to a long duration of the microgravity phase, but high angular change and slow minimum velocity at the top of the parabola. However, low initial velocity makes high angular change impossible. An acceleration of ∼4.5 $g_0$ during the pull-up phase to reach an initial climb angle of ∼50 degrees is a good trade-off. This way it is in principle possible to reach parabola durations of up to 16 s at 0 $g_0$, up to 17 s at 0.17 $g_0$ and up to 21 s at 0.38 $g_0$ with an initial speed of 100 m s$^{-1}$ (Fig. 3).

## The Delta-Wing with Canard Wings

Increasing both, the velocity of the UAV and the payload mass, requires a larger, jet-engine-driven aircraft. The size of the fuselage does not so much depend on the requirement of lift, but on the requirement of payload mass and volume. Thus, we chose as our UAV a delta-wing aircraft with additional canard wings (see Fig. 4). In delta-wing configurations, the fuselage is creating a

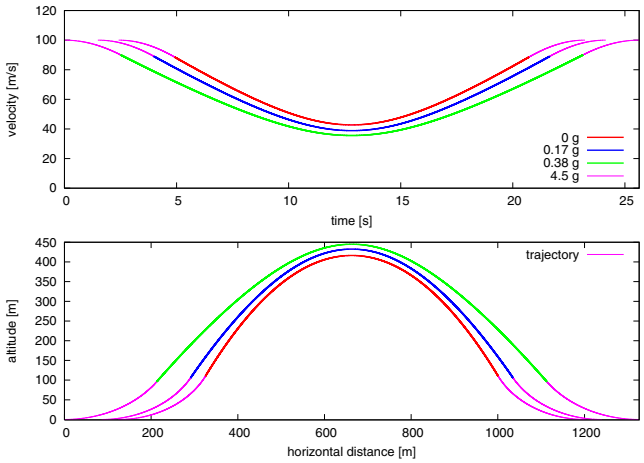


**Fig. 3** Simulated flight paths with an initial velocity of 100 m $s^{-1}$ and a pull-up phase of 2.5 s duration with an acceleration of ~4.5 $g_0$ (*pink* part of the curve). The three fight curves in both diagrams show the velocity (*top*) and altitude (*bottom*) of the aircraft for desired residual accelerations of 0 $g_0$ ("microgravity"; *red*), 0.17 $g_0$ ("lunar gravity"; *blue*), and 0.38 $g_0$ ("Martian gravity"; *green*), respectively

large part of the lift. The fuselage can be rather large to accommodate the low-gravity experiments.

Delta-wing configurations also offer the opportunity to place a large engine in the rear of the aircraft, due to wider limits for the center of gravity (COG), thus using it in a "push" configuration. Single-propeller aircraft in "pull" configuration suffer from the adverse effect that the propwash creates a torque around the vertical yaw axis when it hits the fin of the aircraft. To counter this effect, which is varying throughout the parabola, an additional control system would be required. Aircraft in "push" configuration are not subject to any interaction between the propwash and the body of the aircraft, thus avoiding any unwanted torques.

Due to limited space for experimentation, the COG may shift depending on the experiment. The rear-engine setup ensures a forward shift of the COG to guarantee stable flight regardless of the specific experiment onboard. Especially for ground-controlled flight (where the operator has only limited (visual) feedback of the flight attitude), a forward COG position is favorable. A forward COG helps to damp the pitch and yaw axis, which improves stability during parabolic flight. Canard wings also vastly increase the agility to allow fast turn-around times between multiple parabolas.

## The Engine

The jet engine uses 650 ml fuel (Jet-A1) per minute to create an exhaust speed of 450 m $s^{-1}$ providing a thrust of 180 N. It has a mass of 1.7 kg. Jet engines cause far less vibrations than piston engines and still produce significant thrust at high airspeeds. The engine is manufactured by *Modellturbinen Alfred Frank* and operated by control components from *ProJET electronic components GmbH*. Fuel tanks are implemented as four 750 ml plastic bags in two glass fiber tubes. This effectively prevents running dry during low-*g* flight.


**Fig. 4** Our UAV with a maximum take-off weight of 25 kg, a wingspan of 2 m and a length of 2.5 m, designed for a flight speed of 100 m $s^{-1}$ and an acceleration of 5 $g_0$

The plastic bags are connected to the bottom of a normal 500 ml tank. This tank prevents that air is filled into the plastic bags. During the fuelling procedure, some air is pressed into the de-airing tank. This air moves to the top of the tank where a valve is placed to remove the air from the fuel system before flight. During flight, the de-airing tank is completely filled with fuel. The complete fuel-supply system of our UAV is depicted in Fig. 5. The engine is operated by an electronic control unit, which monitors the temperature and limits the engine speed to 125,000 rpm. During starting, the engine is driven by an electrical motor and fuelled by propane gas. Upon reaching sufficient speed and temperature, the fuel is switched to kerosene. Propane is not available on-board. Therefore mid-air restart is not possible.

## The Controller

The parabolic-flight curves are automated and controlled by the system shown in Fig. 6. For the measurement of the acceleration we used two 2-axis accelerometers (ADXL202 from Analog Devices, http://www.analog.com/en/sensors/inertial-sensors/adxl202/products/product.html) with a sampling rate of 40 Hz and a digitization error of $\lesssim 2 \cot 10^{-3}\ g_0$. The measured vertical acceleration is compared to the set point, and the difference is used by the control unit to minimize the deviation. The control unit consists of a proportional part, an integral part and a differential part. The integral part eliminates the continuous set point deviation. A map-based pre-control is filled with physically expected data and will be tuned by the controller itself (adaptive pre-control). The calculation frequency of the control system is synchronized with the 40 Hz update rate used for the actuator outputs. The response time of the engine is ∼1 s. To minimize the acceleration along the longitudinal axis, a pre-control depending on the measured flight speed is used. The flight speed and its change is used to calculate the drag in the next second by fitting the measured speed to a physically expected function for the speed during the parabola. The required thrust depends on the flight speed and the desired residual acceleration.

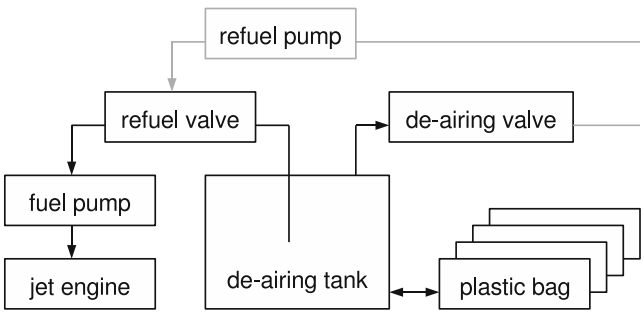


**Fig. 5** The fuel supply system of our UAV

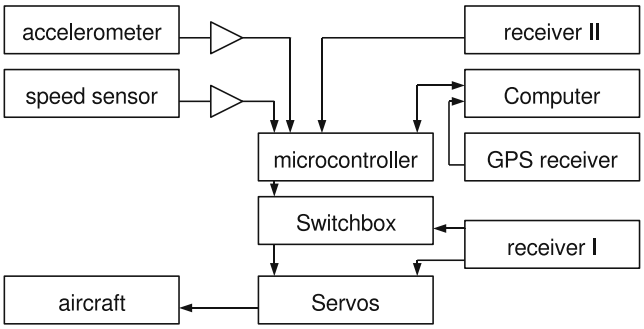


**Fig. 6** The electrical system of our UAV. The accelerometers are two ADXL202 from Analog Devices, http://www.analog.com/en/sensors/inertial-sensors/adxl202/products/product.html, which contain 2 sensors each with a measurement range of $\pm 2\ g_0$. They are sampled at 40 $Hz$

## The Electrical System

The controller is implemented through a software package. Analog signals are amplified before the analog-to-digital conversion to match the range of the analog-to-digital converter and the acceleration sensors. A switchbox allows the operator at the ground to select manual or automatic flight. In case of manual flight, the whole control system is detached from the actuators to minimize possible risk caused by control system failures. Receiver 1, the switchbox and servos are commercial-off-the-shelve components, which have proven functionality in millions of model aircraft. The micro controller (ATMega AVR 32-16) runs at 16 MHz and measures the acceleration and flight speed, thus providing signals to drive the actuators. The computer (200 MHz Intel PXA255, 64 MB SDRAM) operates under linux. It allows fast software development and access to standard media for data storage. No telemetry is used because a single operator cannot supervise telemetry and remote-control the aircraft at the same time, and the risk of dangerous radio interference between transmitted and received data during manual flight is not justified by the benefits. The onboard computer possesses sufficient computing power to perform all necessary calculations so that telemetry for that purpose is also not required.

## Calibration of the Pitot Sensor

To assess the correct airspeed of the aircraft during the parabolic-flight maneuvers, we use a self-made pitot tube sensor, consisting of an aluminum tube with 12 mm

diameter and 150 mm length, with one entrance hole and four side holes. A differential pressure sensor measures the pressure difference between the entrance hole and the four side holes. The pitot tube sensor used for speed measurement was calibrated in the wind tunnel of the *Institute of Fluid Mechanics (TU Braunschweig)* as a basis for tuning of the control system for the acceleration along the longitudinal axis. To guarantee a realistic calibration, the pitot tube sensor was attached to the fuselage so that its air deflection was automatically taken into account.

## Results

Figure 7 shows the airspeed and acceleration during one of the test flights of our UAV, in which we reached a duration of the parabola of ∼12 s, close to the maximum of 16 s. The initial airspeed of our aircraft was 88 m $s^{-1}$ and the pull-up acceleration was well below the maximum possible. The error of the airspeed measurement in Fig. 7 is smaller than the line width; the measurement error of the acceleration is smaller than $2 \cdot 10^{-3}$ $g_0$. The high-frequency changes of the airspeed are caused by different local wind conditions, to which the aircraft could not quickly adjust its absolute airspeed due to inertia. The average vertical acceleration over the time of the parabola is 0.0 $g_0$, and the rms acceleration is 0.4 $g_0$.

The wind conditions differing over the area covered by the parabola do not only affect the airspeed, but the velocity relative to the aircraft orientation in general. Consequently, also the angle of attack differs

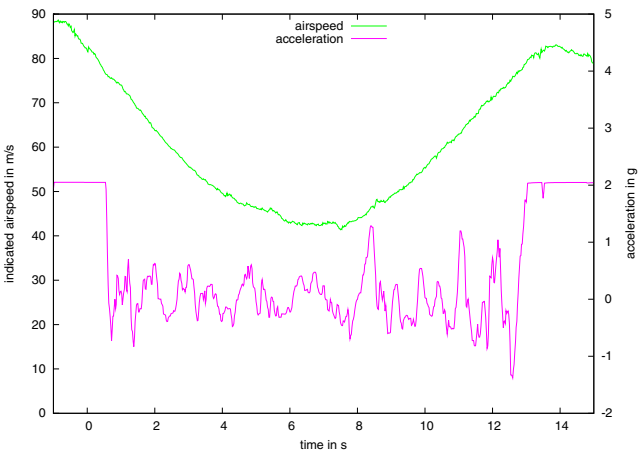


**Fig. 7** Airspeed and acceleration measured during the latest test flight. Significant disturbances were caused by external influences (e.g. at 8 s), Wind conditions were not homogeneous in the area covered by the parabola

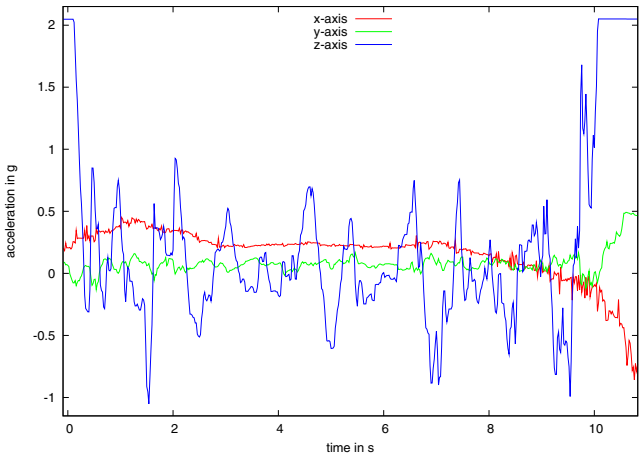


**Fig. 8** Measured accelerations (roll axis x, pitch axis y, and vertical axis z) during one of our test parabolas. Measurement errors are smaller than $2 \cdot 10^{-3}$ $g_0$

depending on the wind conditions, causing changes of the acceleration. The aircraft's ability to achieve the desired acceleration depends on its ability to change the orientation, i.e., on the moment of inertia and the available torque. Due to its small size and mass, the prototype UAV used for the preliminary tests (see Section "Preliminary Tests") had a negligible moment of inertia allowing it to change its orientation extremely quickly without help of any kind of control system. In contrast, the new UAV with a mass of 25 kg and a length of 2.5 m cannot change its orientation quickly enough. This is a major drawback of a somewhat larger UAV as compared to a small aircraft. The user should be aware of this and must weigh this disadvantage against the longer available low-gravity duration.

Figure 8 shows the acceleration along all three axis on the latest flight. Deviations from the desired 0 $g_0$ have mainly two reasons: (1) non-perfectly adapted

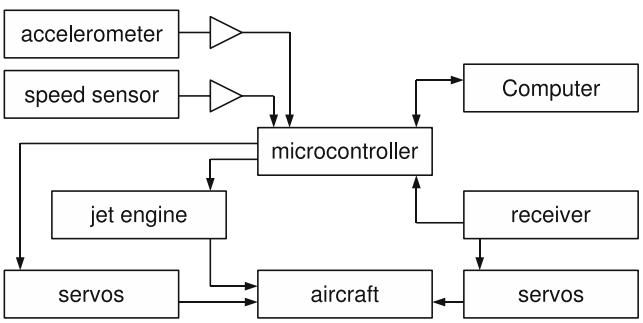


**Fig. 9** The new electrical system of our UAV. Canards and engine will be driven directly by the micro controller. Safe operation is ensured by manual command of the elevons, which allow roll and pitch control

thrust in x direction and (2) "noise" produced by the influence of local winds. At the beginning of the parabola the engine is still producing excessive thrust, resulting in an acceleration along the roll axis x. After the parabola, the engine is no longer producing thrust, causing a negative acceleration in x direction. However, the "noise" of the acceleration in x direction is very small, due to the low influence of wind speed variations on the smallest cross section of the aircraft in x direction. The acceleration along the pitch axis y cannot be influenced by aircraft activities (e.g. thrust and elevators), as the aircraft does not have any related control surface (i.e. a rudder). The rms acceleration along the y axis is in between those of the x and z directions, due to the intermediate surface area of the aircraft against side winds. It is obvious from Fig. 8 that the rms acceleration in z direction is larger than in the other two directions. This is caused by wind variations affecting the largest cross section of the aircraft and cannot easily be reduced.

## Next Steps and Outlook

Having learned from our first parabolic-flight tests, the control system needs be tuned to minimize the acceleration error along the vertical axis. An improved electrical system will be used to support control commands at a higher resolution (Fig. 9). The systematic drift in the acceleration in x direction, visible in Fig. 8, can be significantly reduced by pre-programming a variation in thrust so that thrust excesses will be excluded. Also, some minor hardware modifications will be tested to achieve more stable flight conditions, especially by moving forward the center of gravity.

Due to the finite size of our UAV and its non-negligible mass of almost 25 kg, the aircraft's response to local wind variations cause a typical vibrational level of $\sim$0.4 $g_0$ in z direction, with an overall integrated acceleration of almost perfectly 0 $g_0$. Thus, our UAV is not suited for vibration-sensitive experiments. However, experiments that are insensitive to such vibrational levels can benefit from the low cost of short turnaround times of our small parabolic aircraft.

## References


Beitz, E.: Kollisionen von cm-großen Staubagglomeraten in einem Laborfallturm. Diploma thesis, TU Braunschweig (2010)

Blum, J.: Astrophysical microgravity experiments with dust particles. Microgravity Sci. Technol. **22**, 517–527 (2010)

Dreyer, M.: The drop tower Bremen. Microgravity Sci. Technol. **22**, 461 (2010)

Fitton, B., Seibert, G.: In: A World Without Gravity. In: Fitton, B., Battrick, B. (eds.) Chapter 1: Introduction, pp. 5–34. ESA Publications Division (2001)

Hamacher, H., Fitton, B., Kingdon, J.: The environment of earth-orbiting systems. In: Walter, H.U. (eds.) Fluid Sciences and Material Scieneces in Space, pp. 1–50. Springer (1987)

Jules, K., McPherson, K., Hrovat, K., Kelly, E., Reckart, T.: A status report on the characterization of the microgravity environment of the international space station. Acta Astron. **55**, 335–364 (2004)

Mesland, D.: Ballistocraft: a novel facility for microgravity research. ESA Bulletin, No 82 (1995)

Pletser, V.: Short duration microgravity experiments in physical and life sciences during parabolic flights: the first 30 ESA campaigns. Acta Astron. **55**, 829–854 (2004)

Pletser, V., Pacros, A., Minster, O.: International heat and mass transfer experiments on the 48th ESA parabolic flight campaign of March 2008. Microgravity Sci. Technol. **20**, 177–182 (2008)

Pletser, V., Clervoy, J.-F., Gharib, T., Gai, F., Mora, C., Rosier, P.: Moon and mars gravity environment during parabolic flights: a new European approach to prepare for planetary exploration. Paper No F51-0001-10. In: Proc. of the COSPAR Scientific Assembly 2010. Bremen, Germany. ISSN 1815-2619 (2010)

Rath, H.: Der fallturm bremen als erdgebundenes weltraumlabor für experimente unter kompensierter gravitation. Naturwissenschaften **82**, 117–122 (1995)